

Journal of Materials Chemistry A

Accepted Manuscript



This is an *Accepted Manuscript*, which has been through the Royal Society of Chemistry peer review process and has been accepted for publication.

Accepted Manuscripts are published online shortly after acceptance, before technical editing, formatting and proof reading. Using this free service, authors can make their results available to the community, in citable form, before we publish the edited article. We will replace this *Accepted Manuscript* with the edited and formatted *Advance Article* as soon as it is available.

You can find more information about *Accepted Manuscripts* in the [Information for Authors](#).

Please note that technical editing may introduce minor changes to the text and/or graphics, which may alter content. The journal's standard [Terms & Conditions](#) and the [Ethical guidelines](#) still apply. In no event shall the Royal Society of Chemistry be held responsible for any errors or omissions in this *Accepted Manuscript* or any consequences arising from the use of any information it contains.

Kinetically asymmetric charge and discharge behavior of $\text{LiNi}_{0.5}\text{Mn}_{1.5}\text{O}_4$ at low temperature observed by *in situ* X-ray diffraction

Cite this: DOI: 10.1039/x0xx00000x

Received 00th January 2012,
Accepted 00th January 2012

DOI: 10.1039/x0xx00000x

www.rsc.org/

Ikuma Takahashi,^a Haruno Murayama,^a Kenji Sato,^a Takahiro Naka,^a Koji Kitada,^a Katsutoshi Fukuda,^a Yukinori Koyama,^a Hajime Arai,^a Eiichiro Matsubara,^b Yoshiharu Uchimoto^c and Zempachi Ogumi^a

Capacity decrease at low temperatures is one of the issues to be solved for secondary batteries especially for automobile applications and it is thus important to clarify the reaction kinetics in operating batteries and identify the rate determining step that governs the performance at low temperatures. Phase transitions in electrode active materials are important factors that affect the reaction kinetics particularly for thin electrodes used in high power applications. In this study, the phase transition dynamics of thin $\text{LiNi}_{0.5}\text{Mn}_{1.5}\text{O}_4$ electrodes at various temperatures is examined using electrochemical methods combined with temperature-controlled *in situ* X-ray diffraction analysis to directly capture the reacting species and elucidate reaction mechanism. The analysis shows that there occur consecutive phase transitions of $\text{LiNi}_{0.5}\text{Mn}_{1.5}\text{O}_4$ (Li1 phase) \leftrightarrow $\text{Li}_{0.5}\text{Ni}_{0.5}\text{Mn}_{1.5}\text{O}_4$ (Li0.5 phase) and the Li0.5 phase \leftrightarrow $\text{Ni}_{0.5}\text{Mn}_{1.5}\text{O}_4$ (Li0 phase) at room temperatures and above. At lower temperatures the transition of Li1 \rightarrow Li0.5 proceeds during the charging process but further delithiation to form the Li0 phase is restricted, leading to the capacity decrease. On the other hand on discharging at low temperatures the amount of the Li0 phase to be lithiated is limited and this causes the capacity decrease. There is no Li0.5 phase formation on discharging at low temperatures, revealing remarkable kinetic asymmetry of the reaction processes for charging and discharging. It is suggested that the Li0.5 phase formed on discharging is instantly lithiated to form the Li1 phase, due to the small potential gap between the two transitions. These results indicate that the phase transition kinetics of Li0.5 \leftrightarrow Li0 is slower than that of Li1 \leftrightarrow Li0.5 and the former transition is the rate determining step at low temperatures.

1. Introduction

Lithium ion batteries have been widely used as power sources for portable devices and now become to be used for electric vehicles (EVs) and hybrid electric vehicles (HEVs). It is required for batteries to keep their performances such as discharge capacity, power and durability in various operating conditions and this is particularly important for these vehicle applications. As for the temperature, the operating range of the vehicles can be as wide as from $-20\text{ }^\circ\text{C}$ to $60\text{ }^\circ\text{C}$, which is a demanding condition for the batteries. Significant capacity dependence of the batteries on the operating temperature has been reported¹⁻³ and a decrease in the capacity at low temperatures is known to be a particularly serious problem. Such behavior should be improved, nevertheless, it is difficult to clarify the origin of the capacity decrease because there are several possible rate determining steps in the battery reactions and the most important step can change depending on the battery configuration and the operating environment. The rate determining step is often the ion transportation in the electrode immersed in the electrolyte for high

capacity batteries with thickly coated electrodes such as those for EVs⁴⁻⁶, while the phase transitions in the electrode active material can be the rate determining step for high power batteries with thin electrodes such as those used in HEVs.⁷ In the latter case, direct observation of the reacting species in the electrode during the electrochemical reactions is essential and so experimental methods such as *in situ* X-ray diffraction (XRD) are promising.

$\text{LiNi}_{0.5}\text{Mn}_{1.5}\text{O}_4$ with a spinel structure is known to show high energy density with high operating potential.^{8,9} It has been also recognized that the disordered polymorph (space group $\text{P4}_3\text{32}$), in which nickel and manganese randomly occupy the octahedral sites,⁹ shows high rate capability, making this compound an attractive electrode active material especially for HV applications. In the charge-discharge processes there are low and high potential plateaus at around 4.7 V vs. Li/Li^+ ^{10,11} that correspond to the phase transitions of $\text{LiNi}_{0.5}\text{Mn}_{1.5}\text{O}_4$ (Li1 phase) \leftrightarrow $\text{Li}_{0.5}\text{Ni}_{0.5}\text{Mn}_{1.5}\text{O}_4$ (Li0.5 phase) and of $\text{Li}_{0.5}\text{Ni}_{0.5}\text{Mn}_{1.5}\text{O}_4$ (Li0.5 phase) \leftrightarrow $\text{Ni}_{0.5}\text{Mn}_{1.5}\text{O}_4$ (Li0 phase), respectively.¹²⁻¹⁴ It has been shown that for thin electrodes the solid phase transition is actually the rate determining step and the

phase transition kinetics considerably affects the electrode performance.¹⁵ Because kinetic behavior is generally influenced by temperatures, it is expected that clarifying the phase transitions behavior at various temperatures can give insight to the reaction mechanism and is useful in view of both scientific knowledge and practical applications.

In this paper we report the crystal structural changes of $\text{LiNi}_{0.5}\text{Mn}_{1.5}\text{O}_4$ electrodes by using the temperature controlled *in situ* XRD with high time resolutions to examine their dynamic behavior. The behavior of the Li1, Li0.5 and Li0 phases captured by the *in situ* XRD method is used to elucidate the reaction dynamics. The origin of the capacity decrease at low temperatures and marked kinetically asymmetric charge/discharge behavior are shown, together with possible reaction mechanisms.

2. Experimental

2.1 Sample preparation

The working composite electrode consisted of powder of $\text{LiNi}_{0.5}\text{Mn}_{1.5}\text{O}_4$ (Toda Kogyo) classified under 15 μm , acetylene black as a conductive additive and polyvinylidene difluoride as a binder, mixed in a 80:15:5 wt% ratio and coated on an aluminum current collector. Using neutron diffraction (not shown), this $\text{LiNi}_{0.5}\text{Mn}_{1.5}\text{O}_4$ powder is categorized as the disordered phase.¹⁵ The thickness of the working electrode was about 25 μm to minimize the resistance associated with ion transportation in the electrolyte contained in the electrode. The aluminum pouch-type cell used for the *in situ* measurements consisted of a working electrode (30 mm by 15 mm), metallic lithium foil as counter and reference electrodes, and a 1 mol dm^{-3} LiPF_6 solution of ethylene carbonate and ethylmethyl carbonate (3:7) as the electrolyte. A polyolefin film was used as a separator.

2.2 Electrochemical measurement

The temperature-controlled electrochemical measurements were employed at -20, -10, 0, 10, 25, and 40 °C. We used constant current and potential step experiments to see the dynamic behavior of the electrode material. Constant current conditions were adopted at 1C rate between the potential ranges of from 3.50 V to 4.85 V vs. Li/Li^+ . As to the potential step conditions, the cell potential was stepped from 4.59 V to 4.85 V and kept at 4.85 V for 1800 s in charging, while it was stepped from 4.85 V to 4.59 V and kept at 4.59 V for 1800 s in discharging. Here, assuming that 4.72 V is the potential where the Li0.5 phase is thermodynamically stable¹⁵, we set 4.85 V and 4.59 V (both 0.13 V apart from 4.72 V) as the potential values where the Li0 and Li1 phases are thermodynamically stable, respectively. Potential higher than 4.85 V was avoided to minimize undesirable electrolyte oxidation reactions. The initial status was set from the fully discharged state (obtained by 0.1C discharging to 3.50 V) with a constant charging current flow at 0.1C rate at room temperature before the potential step experiments at various temperatures.

2.3 *In situ* X-ray diffraction measurement

In situ XRD was performed in a transmission mode with an electrochemical cell set in a temperature controlled jacket at BL28XU of SPring-8, Hyogo, Japan. The incident X-ray of 12.4 keV with a wavelength of $\lambda = 0.100$ nm was used with its beam size of 1.0 mm by 0.3 mm. A two dimensional detector PILATUS was set at near $2\theta = 37^\circ$, and we measured the (115) diffraction peak of $\text{Li}_x\text{Ni}_{0.5}\text{Mn}_{1.5}\text{O}_4$. The (115) diffraction was selected to clearly see the transient behavior since there is no other diffraction from the cell

components such as aluminum in this diffraction region. The diffraction pattern was measured in 0.5 s with the interval of another 8 s.

3. Results and discussion

3.1 Electrochemical behavior under constant current conditions

Fig. 1 shows the charge curves of $\text{LiNi}_{0.5}\text{Mn}_{1.5}\text{O}_4$ at 1C rate measured at various temperatures. As the temperature becomes low,

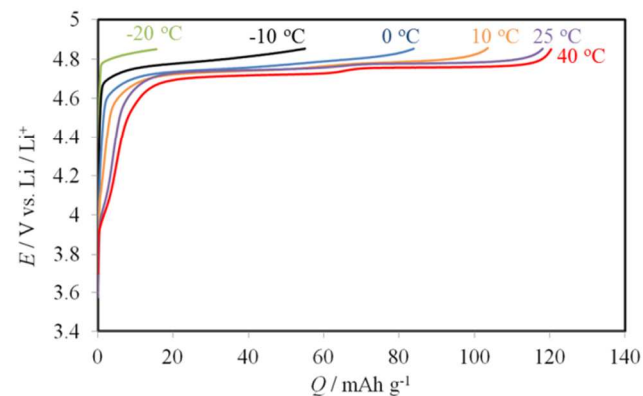


Fig. 1 Charge curves of $\text{LiNi}_{0.5}\text{Mn}_{1.5}\text{O}_4$ at 1C rate in potential range from 3.50 to 4.85 V measured at various temperatures.

the capacity significantly decreases. The capacity at -20 °C and that at -10 °C are respectively about 1/6 and 1/2 of that at 25 °C. The two plateaus are clearly visible at 25 °C while the shape of the potential profile seems to be monotonous at -10, 0 and 40 °C. To clearly see the features of the potential profiles, the derivative values of the capacity Q per potential E , dQ/dE , are plotted versus E for the charge curves measured at -10, 0 and 40 °C as shown in Fig. 2. Here

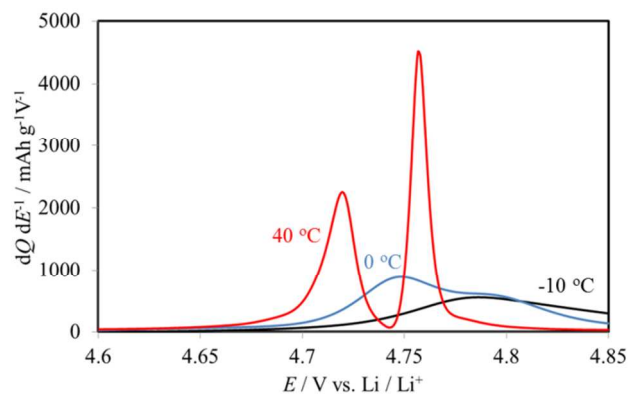
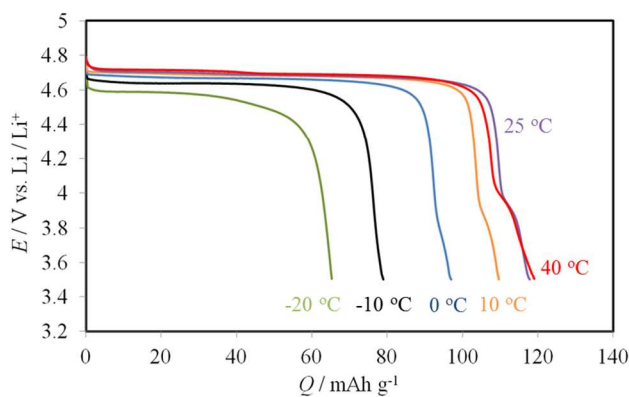


Fig. 2 dQ/dE plots of 1C charge curves of $\text{LiNi}_{0.5}\text{Mn}_{1.5}\text{O}_4$ measured at -10, 0 and 40 °C.

a plateau in a potential profile is shown as a peak in the derivative plot. Two sharp peaks are observed at 40 °C while two peaks are broaden and overlapped at 0 °C, and only a single peak is found at -10 °C.

Fig. 3 shows the discharge curves measured at various temperatures. The capacity dependence on the temperature for the discharge process is less than that for the charge process, and the 1C discharge capacity at -20 °C is about half of that at 25 °C, which is larger than the case observed for charging. To detail the features of

the discharging potential profiles, the dQ/dE plots at -10, 0 and 40 °C



potential range from 4.85 to 3.5 V measured at various temperatures.

are shown in Fig. 4. As shown, two sharp peaks are observed at 40 °C while a single peak is observed at low temperatures. However, the shape of the peak is still sharp, unlike that observed during charging.

For a composite electrode with carbon additives to enhance the electronic conductivity, the rate determining step of an electrode reaction is generally either the ion transportation through the electrolyte region or the ion diffusion/phase transition in the electrode material. In our case both the capacities and the profiles at the same rate considerably differ for charging and discharging, suggesting that the ion transportation through the electrolyte region, which is expected to be identical for charging and discharging, is not the rate determining step. For the $\text{LiNi}_{0.5}\text{Mn}_{1.5}\text{O}_4$ electrode that shows two-phase coexistence regions, it is deduced that one of the phase transitions involved in the delithiation/lithiation processes is the rate determining step.

The two dQ/dE peaks observed for the profiles measured at 40 °C can be assigned to the two phase transitions of the Li0 phase \leftrightarrow the Li0.5 phase and the Li0.5 phase \leftrightarrow the Li1 phase.^[10,11] At low temperature there seem to be a single peak for both the charge and discharge processes. However it is difficult to assign each single peak to one of the two phase transitions or to a united peak for two transitions with only the electrochemical techniques, due to the small potential gap between the two transitions. To understand the behavior, it is important to directly capture the species of interest and

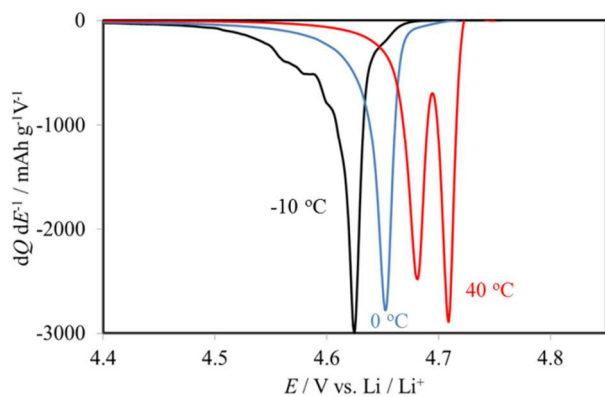


Fig. 4 dQ/dE plots of 1C discharge curves of $\text{LiNi}_{0.5}\text{Mn}_{1.5}\text{O}_4$ measured at -10, 0 and 40 °C.

its dynamic changes brought by the electrochemical processes.

3.2 Phase transition behaviour during charging observed by *in situ* XRD measurements

We thus observed the phase transition behavior using *in situ* XRD measurements that can track the dynamic behavior of the reacting Li1 , Li0.5 and Li0 phases. Here we used potential step methods for electrochemical perturbation instead of constant current charging/discharging because the event is shown as a function of time with the potential step method and this gives information on the reaction kinetics. The terminal potential values were set at 4.85 V and 4.59 V where only the Li0 and Li1 phases are thermodynamically stable, respectively. For the potential step charging experiment to 4.85 V, it is expected that both phase transitions of $\text{Li1} \rightarrow \text{Li0.5}$ and $\text{Li0.5} \rightarrow \text{Li0}$ consecutively occur.

Fig. 5 gives the capacity versus time by the potential step experiment in charging. Denoting the capacity at 25 °C ($Q_{25\text{°C}}$, ca. 110 mAh g^{-1}) as the nominal capacity, the measured capacity on the

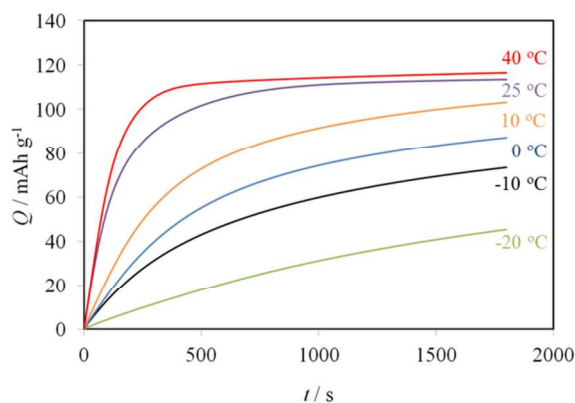


Fig. 5 Capacity curves of $\text{LiNi}_{0.5}\text{Mn}_{1.5}\text{O}_4$ versus time by potential step charge from 4.59 to 4.85 V measured at various temperatures.

basis of the nominal capacity (capacity ratio: $Q_T/Q_{25\text{°C}}$ %) is approximately 100% at 40 °C, 70 % at 0 °C and 50% at -10 °C at the end of 1800 s charging. Fig. 6 shows the result of the time-resolved *in situ* XRD during the potential step charging at 40 °C. As shown in

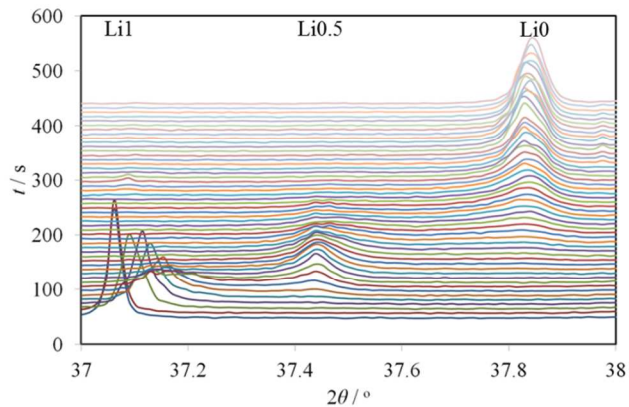


Fig. 6 Time-resolved *in situ* XRD patterns by potential step charge from 4.59 to 4.85 V measured at 40 °C.

this figure, three peaks corresponding to the Li1, Li0.5 and Li0 phases were observed during the charging process, corresponding to the transition from the Li1 phase to the Li0.5 phase and that from the Li0.5 phase to the Li0 phase in two phase coexistence manners. This reaction process coincides with the previous reports on *in situ* XRD measurements.^{14, 15} To visually show the phase transition behavior, the obtained XRD patterns were transformed into graphic images as shown below, with their intensity being shown as different color.

Figs. 7 (a), (b) and (c) show the images of the *in situ* time-resolved XRD patterns measured during the potential step charging at 40, 0, -10 °C, respectively. At 40 °C, the initial Li1 phase almost completely

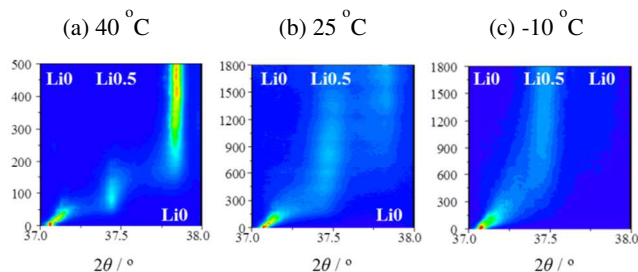


Fig. 7 Time-resolved *in situ* XRD pattern images by potential step charge from 4.59 to 4.85 V measured at (a) 40, (b) 0 and (c) -10 °C.

changes to the Li0 phase via the Li0.5 phase in 400 s after the potential step. This is in good agreement with the result shown in Fig. 5, namely, the charge capacity reaches approximately 95% of the nominal capacity in 400 s after the potential step. On the other hand, at 0 °C, the transition to the Li0.5 phase is nearly terminated and the transition to the Li0 phase starts in 600 s after the potential step, as shown in Fig. 7 (b). In 1800 s after the potential step, there are nearly the same amounts of the Li0.5 and Li0 phases. These results correspond to the charge capacities at 0 °C shown in Fig. 5 of approximately 50% and 70% of the nominal capacity in 600 s and 1800 s after the potential step, respectively. At further low temperature of -10 °C, there is no Li0 phase formation and the Li0.5 phase still remains even after 1800 s as shown in Fig. 7 (c). The charged capacity is a half of the nominal capacity and so only the phase transition from the Li1 phase to the Li0.5 phase proceeded in 1800 s at -10 °C, though the potential value is set at 4.85 V where only the Li0 phase is thermodynamically stable.

To summarize the results obtained in the charging experiments, the formation of the Li0 phase via the Li0.5 phase proceeds at higher temperatures while the reaction stops with the Li0.5 phase formation presumably because the phase transition of Li0.5 → Li0 is kinetically slow (i.e., the rate determining step) and this causes the capacity decrease at low temperatures during the charging process.

3.3 Phase transition behaviour during discharging observed by *in situ* XRD measurements

For the discharging experiments, the potential was stepped from 4.85 V to 4.59 V so that both phase transitions of Li0 → Li0.5 and Li0.5 → Li1 consecutively occur. Fig. 8 shows the obtained capacity versus time during the potential step discharging experiment. The relative capacity of Q_t/Q_{250C} by the potential step is approximately 100 % at 40 °C, 80% at 0 °C and 55% at -10 °C at the end of 1800 s discharging while the nominal capacity Q_{250C} values are nearly the same for charging and discharging. Being similar to the case of the 1C rate tests, the obtained capacity dependence on the temperature is

different for charging and discharging, showing kinetic asymmetry

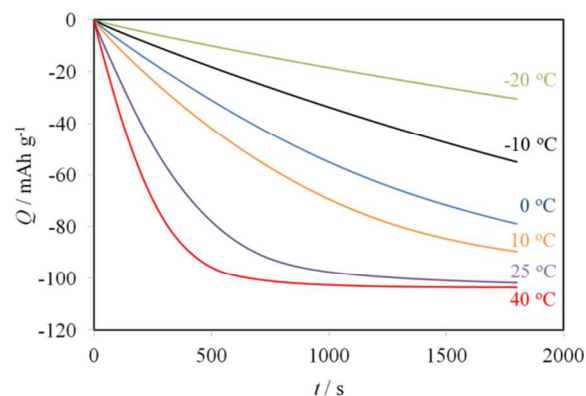


Fig. 8 Capacity curves of $\text{LiNi}_{0.5}\text{Mn}_{1.5}\text{O}_4$ versus time by potential step discharge from 4.85 to 4.59 V measured at various temperatures.

in the electrode reaction process.

To track the dynamic structural changes during the potential step discharging, the *in situ* time-resolved XRD measurements were conducted at 40, 0, and -10 °C and the results are respectively shown in Figs. 9 (a), (b) and (c). At 40 °C, all the Li0, Li0.5 and Li1 phases are observed and the transition seems to be terminated in 500 s after the potential step discharging. This is in good agreement with the capacity shown in Fig. 8 reaching approximately 95% of the nominal capacity in 500 s. Though there appears the Li0.5 phase as the

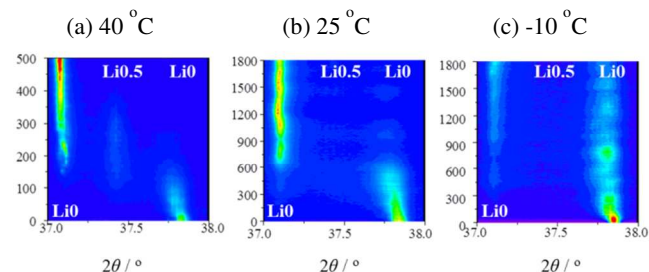


Fig. 9 Time-resolved *in situ* XRD pattern images by potential step discharge from 4.85 to 4.59 V as discharge at (a) 40, (b) 0 and (c) -10 °C.

intermediate species during discharging, the intensity is much weaker than that observed during charging. This is probably because the phase transition of Li0.5 → Li1 is faster than that of Li0 → Li0.5 and the former transition to occurs before the Li0.5 phase constitutes an XRD coherent (long-range ordered) domain. Nevertheless, the phase transitions basically proceed via the Li0.5 phase in a stepwise manner.

Fig. 9 (b) shows that at 0 °C the Li0.5 phase cannot be observed and the Li0 phase partially remains even in 1800 s after the potential step. This seems to correspond to that the discharge capacity is approximately 80% of the nominal capacity at 0 °C (see Fig. 8), leaving 20% of the Li0 phase unchanged. In case of the measurement at -10 °C, no peak for the Li0.5 phase is observed and in 1800 s after the potential step the peak intensity of the Li0 phase still strongly remains, which seems to be equivalent to that of the Li1

phase. This corresponds to the discharge capacity at $-10\text{ }^{\circ}\text{C}$ being about a half of the nominal capacity.

The absence of the Li0.5 phase during discharging at $0\text{ }^{\circ}\text{C}$ and $-10\text{ }^{\circ}\text{C}$ is totally different from the behavior observed during charging, clearly showing the kinetic asymmetry of the system. The reason for the capacity decrease at low temperatures during potential step discharging is ascribed to that the phase transition of $\text{Li0} \rightarrow \text{Li0.5}$ is the rate determining step and only a part of the Li0 phase is lithiated. It is deduced that, once the Li0.5 phase is formed, it is quickly lithiated to form the Li1 phase, resulting in the absence of the Li0.5 phase in the XRD measurement at low temperatures.

3.4 Phase transition behaviour associated with 1C rate experiments

The reaction mechanism observed in the 1C rate constant current experiments shown in Figs. 1 to 4 are now elucidated based on the results obtained in the potential step experiments with *in situ* XRD measurements. The trends of the capacity dependence on the temperature are similar for both the 1C rate constant current experiments and potential step experiments, regardless of the current direction (charging or discharging), see Fig. 1 with Fig. 5 and Fig. 3 with Fig. 8. Based on this, the characteristics of the dQ/dE profiles at various temperatures can be interpreted using the results obtained by the *in situ* XRD measurements. The two sharp peaks of the dQ/dE plot at $40\text{ }^{\circ}\text{C}$ shown in Fig. 2 correspond to the transitions of $\text{Li1} \rightarrow \text{Li0.5}$ at low potential and $\text{Li0.5} \rightarrow \text{Li0}$ at high potential. At $0\text{ }^{\circ}\text{C}$ the dQ/dE peaks are broaden, reflecting the slow reaction kinetics. The peak area corresponding to the transition of $\text{Li0.5} \rightarrow \text{Li0}$ at higher potential is small because the Li0.5 phase partially remains. At $-10\text{ }^{\circ}\text{C}$, a single broad peak of dQ/dE is considered to correspond to the phase transition of Li1 phase $\rightarrow \text{Li0.5}$. For the discharging process, the two dQ/dE peaks observed at $40\text{ }^{\circ}\text{C}$ in Fig. 4 correspond to the transitions of $\text{Li0} \rightarrow \text{Li0.5}$ at high potential and $\text{Li0.5} \rightarrow \text{Li1}$ at low potential. On the other hand, the apparent single peak observed at $0\text{ }^{\circ}\text{C}$ and $-10\text{ }^{\circ}\text{C}$ can be ascribed to the phase transition of $\text{Li0} \rightarrow \text{Li1}$, which is a combination of the transitions of $\text{Li0} \rightarrow \text{Li0.5}$ and $\text{Li0.5} \rightarrow \text{Li1}$. The apparent electrochemical behavior is similar each other for charging and discharging, nevertheless, the actual reactions occurring in the electrode are different. This could affect other properties of the electrode, for example safety at the same state of charge.

The phase transition kinetics of $\text{Li0} \leftrightarrow \text{Li0.5}$ being slower than that of $\text{Li1} \leftrightarrow \text{Li0.5}$ is particularly conspicuous at low temperatures, suggesting that the activation energy barrier for the former transition is higher than that for the latter transition. The kinetic study to reveal the activation energy will give detailed information on the reaction mechanism, which is an interesting future topic. It is noted that the involved three phases have the same spinel-based structures, though there is remarkable kinetic difference between these two transitions. A possible reason for the difference is that the Li1 phase has a solid solution region as shown in Fig. 6 that can mitigate the volume change between the Li1 and Li0.5 phases and facilitate the transition of $\text{Li1} \leftrightarrow \text{Li0.5}$. The volume change through the transition could also affect, namely, a 3.3% change for $\text{Li0} \leftrightarrow \text{Li0.5}$ and a 2.9% change for $\text{Li1} \leftrightarrow \text{Li0.5}$. It is also noted that these *in situ* analyses of the electrode reaction dynamics are expected to be useful for optimizing electrode performances by, for example, controlling the charge/discharge conditions and the particle size of the material.

4. Conclusions

Temperature controlled *in situ* XRD measurements are useful for clarifying the reaction dynamics of electrode materials during charging and discharging at various temperatures and elucidate the

mechanism for the capacity dependence on the temperature. For $\text{LiNi}_{0.5}\text{Mn}_{1.5}\text{O}_4$ electrodes, the phase transition kinetics of $\text{Li1} \leftrightarrow \text{Li0.5}$ and $\text{Li0.5} \leftrightarrow \text{Li0}$ are similar and the three phases consecutively appear at room temperature and above. At low temperatures the transition $\text{Li0.5} \leftrightarrow \text{Li0}$ is kinetically slow and becomes the rate determining step, resulting in the capacity decrease by restricting the formation of the Li0 phase (with remaining unreacted Li0.5 phase) for the charging process and by limiting the amount of the Li0 phase that are lithiated (with leaving unreacted Li0 phase) for the discharging process.

As described in the case of $\text{LiNi}_{0.5}\text{Mn}_{1.5}\text{O}_4$, thermodynamically reversible electrode systems can behave kinetically asymmetrically during charging and discharging, and it is thus important to use *in-situ* technique to elucidate the reaction mechanism, in addition to the electrochemical methods. In particular, synchrotron beam aided analysis with a high time resolution is promising to track fast reactions. The information obtained with the *in situ* measurements is practically useful for designing electrodes and setting charge/discharge conditions to realize high performance of the batteries.

Acknowledgements

This work was supported by Research and Development Initiative for Scientific Innovation of New Generation Batteries (RISING) project of NEDO (Japan). The synchrotron radiation experiments were performed with the approval of the Japan Synchrotron Radiation Research Institute (JASRI) (Proposal No. 2010B1896, 2011A1013, 2011A1014, 2011B1034, 2012A7601, 2012B7601).

Notes and references

^a Office of Society-Academia Collaboration for Innovation, Kyoto University, Gokasho, Uji, 611-0011, Japan

^b Department of Materials Science & Engineering, Kyoto University, Yoshida-Honmachi Sakyo-ku, Kyoto, 606-8501, Japan

^c Graduate School of Human and Environmental Studies, Kyoto University, Sakyo-ku, Kyoto, 606-8501, Japan

- X.-Z. Liao, Z.-F. Ma, Q. Gong, Y.-S. He, L. Pei, L.-J. Zeng, *Electrochem Commun.* 2008, **10**, 691.
- Z. Li, Y. Wang, X. Bie, K. Zhu, C. Wang, G. Chen, Y. Wei, *Electrochem Commun.* 2011, **13**, 1016.
- W.C. West, J. Soler, M.C. Smart, B.V. Ratnakumar, S. Firdosy, V. Ravi, M.S. Anderson, J. Hrbacek, E.S. Lee, A. Manthiram, *J. Electrochem. Soc.* 2011, **158** A833.
- A.-K. Hjelm, G. Lindbergh, *Electrochim Acta.* 2002, **47**, 1747.
- M.D. Levi, D. Aurbach, *J. Power Sources.* 2005, **146**, 727.
- D. Dees, S. Kawauchi, D.P. Abraham, J. Prakash, *J. Power Sources.* 2009, **189**, 263.
- D. Lu, W. Li, X. Zuo, Z. Yuan, Q. Huang, *J. Phys. Chem. C.* 2007, **111**, 12067.
- Q. Zhong, A. Bonaklapour, M. Zhang, Y. Gao, J.R. Dahn, *J. Electrochem. Soc.* 1997, **144**, 205.
- J.-H. Kim, S.-T. Myung, C.S. Yoon, S.G. Kang, Y.-K. Sun, *Chem. Mater.* 2004, **16**, 906.
- K. Dokko, M. Mohamedi, N. Anzue, T. Itoh, I. Uchida, *J. Mater. Chem.* 2002, **12**, 3688.
- D.H. Park, S.T. Lim, S.-J. Hwang, J.-H. Choy, J.H. Choi, J. Choo, *J. Power Sources*, 2006, **159**, 1346.
- M. Kunduraciz, G.G. Amatucci, *Electrochim Acta.* 2008, **53**, 4193.
- L. Wang, H. Li, X. Huang, E. Baudrin, *Solid State Ionics.* 2011, **193**, 32.
- K. Rhodes, R. Meisne, Y. Kim, N. Dudney, C. Daniel, *J. Electrochem. Soc.* 2011, **158**, A890.

- 15 H. Arai, K. Sato, Y. Oriasa, H. Murayama, I. Takahashi, Y. Koyama, Y. Uchimoto, Z. Ogumi, *J. Mater. Chem. A*, 2013, **1**, 10442.